Nanoscale Advances

ROYAL SOCIETY OF CHEMISTRY

COMMUNICATION

View Article Online
View Journal | View Issue

Cite this: *Nanoscale Adv.*, 2026, **8**, 3131

Received 5th February 2026
Accepted 22nd April 2026

DOI: 10.1039/d6na00092d

rsc.li/nanoscale-advances

Structure-mediated fluid-involved behaviors promote the performance of a carbon-based supercapacitor

Heping Cao,†[ab] Chengqing Tang,†[ac] Jiashuo Duan,[a] Zhaohui Yang *[b] and Yitan Li *[acd]

Carbon nanotube sponges (CNTSs), a promising electrode material, are limited by inherent hydrophobicity. Herein, various TiO_2 nanostructures were synthesized inside CNTSs, providing pseudocapacitance and regulating the wettability and ion migration of the electrolyte, thereby enhancing the area-specific capacitance by up to 250%. These results offer insights into advanced energy storage systems.

Supercapacitors have attracted wide attention for their high power density,[1,2] fast charging–discharging rate with high current density,[3,4] long cycle life[5,6] and safety,[7,8] and they are considered to be promising candidates for use in next-generation energy storage systems.[9–12] The performance of a supercapacitor is mainly governed by the characteristics of the electrode material (specific surface area, pore structure, and conductivity) and those of the electrolyte (ionic conductivity and electrochemical performance), and the compatibility between them.[13,14] Notably, the behavior of the electrolyte within the electrode structure plays a non-negligible role.[15,16] From a surface chemistry perspective, sufficient wetting of the electrode surface by the electrolyte is required to ensure an adequate solid–liquid contact area.[17] This is essential for forming the electric double layer[18] and facilitating electrochemical reactions.[19] Furthermore, the migration mode of ions within the electrolyte directly determines the ion transport kinetics, thereby influencing the overall performance of the supercapacitor.[20,21] Insufficient ion migration under high-rate conditions leads to a decline in capacitive performance during rapid charge–discharge cycles.[22,23] Therefore, developing materials possessing high porosity, a large specific surface area, efficient ion transport pathways, and suitable electrolyte wettability is of paramount importance.[14,24,25]

Carbon nanotube sponges (CNTSs) are a class of conductive aerogel composed of multi-walled carbon nanotubes, offering multiple advantages.[26–28] The self-supporting conductive network formed by interconnected carbon nanotubes provides an exceptionally high specific surface area and abundant mesopores. These structural features facilitate electrolyte infiltration and rapid ion transport, thereby enhancing power density. Moreover, the network ensures excellent electron conduction pathways and mechanical resilience.[29,30] However, it is important to note that pristine CNTSs, when used as a supercapacitor electrode, possess inherent limitations. These include a relatively monodisperse pore structure, a single charge storage mechanism (EDLC), and poor surface wettability (as, due to the highly non-polar nature of the graphitic carbon surfaces, they exhibit strong inherent hydrophobicity), all of which can restrict their charge storage capability.[31,32] It remains a significant yet challenging task to modify the interfacial properties of CNTSs without compromising their inherent structural and performance benefits.[33]

Here in this study, TiO_2 nanostructures with different morphologies were introduced into CNTS *via* a facile hydrothermal method, forming spherical, urchin-like, and thorn-like TiO_2@CNTS composites. Experimental and simulation results demonstrate that, compared to pristine CNTS, these TiO_2 nanostructures not only enhance electrolyte wettability but also provide additional effective solid–liquid interfaces for energy storage. The area-specific capacitance values of the TiO_2@CNTS composites exhibited significant increases of 196.4%, 204.8%, and 250% for the spherical, urchin-like, and thorn-like TiO_2 nanostructures, respectively, where the thorn-like TiO_2@CNTS composite exhibits the maximal improvement in performance. This work highlights the correlation between electrolyte

[a]*National Engineering Research Center for Colloidal Materials, School of Chemistry and Chemical Engineering, Shandong University, Jinan, Shandong, 250100, P. R. China. E-mail: yitanli@sdu.edu.cn*

[b]*School of Physical Science and Technology, Soochow University, Suzhou, 215006, P. R. China. E-mail: yangzhaohui@suda.edu.cn*

[c]*Intelligent Chemical Engineering Center, Hong Kong Research Institute of Shandong University, Hong Kong SAR, P. R. China*

[d]*Suzhou Research Institute, Shandong University, Suzhou, Jiangsu, 215123, P. R. China*

† These authors contributed equally to this work.

infiltration behavior and TiO_2 morphology, providing insights into the design of next-generation supercapacitors.

By tuning the conditions during hydrothermal synthesis, spherical, urchin-like, and thorn-like TiO_2 nanostructures were synthesized on carbon nanotube sponges (CNTSs) obtained by the chemical vapor deposition (CVD) method.

In typical synthesis processes, the morphology of TiO_2 nanostructures evolved from spherical to urchin-like as the concentration of HCl increased from 2 mL to 8 mL at low titanium precursor concentrations of 100 to 500 μL. Conversely, TiO_2 is more likely to form bulk and thorn-like structures at a higher titanium precursor concentration of 700 μL, while simultaneous increases of both precursor and HCl concentrations lead to TiO_2 spheres (Fig. 1). The morphological evolution can be ascribed to the fact that the carbon nanotubes serving as a self-supporting framework provide abundant heterogeneous nucleation sites. The precursor concentration determines the initial nucleation density by controlling supersaturation, while hydrochloric acid acts as a kinetic inhibitor, modulating the hydrolysis rate of Ti^{4+} and promoting anisotropic growth along the (001) direction through selective adsorption onto specific crystal facets. This synergistic effect between the precursor and acid concentrations leads to a structural transition from sparse spherical shapes to dense urchin-like structures, and finally to a bulk-like architecture, which is consistent with previously reported growth mechanisms.[34]

The hydrothermal approach enables the *in situ* growth of TiO_2 nanostructures on carbon nanotubes. Taking spherical TiO_2@CNTS as an example, the TiO_2 particles grown directly on CNTS form a "string-of-pearls" architecture, demonstrating robust interfacial bonding and sufficient contact between the nanostructures and CNTS, indicating superior electrical conductivity and mechanical stability. Moreover, spherical TiO_2@CNTS exhibited a contact angle of 27° (Fig. S3b), which is much lower than the value of 98° for pristine CNTS. Urchin-like TiO_2@CNTS and thorn-like TiO_2@CNTS also exhibited excellent electrolyte wettability, suggesting a potential increase in the charge storage capability of TiO_2@CNTS-based supercapacitors.

Energy dispersive X-ray spectroscopy (EDS) mapping and X-ray diffraction (XRD) pattern results confirm the TiO_2@CNTS structures (Fig. 2a and b). The characteristic peaks of the hydrothermally synthesized rutile TiO_2 are clearly identified at 26.7° (110), 36.12° (101), 44.08° (111), 56.68° (211), and 69.80° (332).[35] The characteristic peak of CNTS appears at 26.7°, corresponding to the (002) plane of graphitic carbon. All three TiO_2 nanostructures possess a rutile crystalline phase. The resistances of TiO_2@CNTS are 0.103 kΩ m^{-1} (spherical TiO_2@CNTS composite), 0.106 kΩ m^{-1} (urchin-like TiO_2@CNTS composite), and 0.116 kΩ m^{-1} (thorn-like TiO_2@CNTS composite). The introduction of TiO_2 nanostructures not only improved the wettability but also mediated ion flow inside the TiO_2@CNTS composites. A laminar flow model was established in COMSOL, with the necessary hydrodynamic and physical parameters such as material type, viscosity coefficient, conductivity, and Young's modulus carefully defined. It can be observed that the ion flow velocity is maximized in the central regions of the pores and decreases near the particle edges due to fluid viscosity effects. Compared to spherical and urchin-like samples, the thorn-like TiO_2@CNTS material possesses a more developed nanoscale pore structure, providing a greater number of transport pathways for ion adsorption and desorption near the electrode surface. Moreover, the interfacial integral length of thorn-like TiO_2@CNTS is 1588.4 μm, which is 4 times that of spherical TiO_2@CNTS and 2 times that of urchin-like TiO_2@CNTS. The larger solid–liquid contact area also ensures the maximum

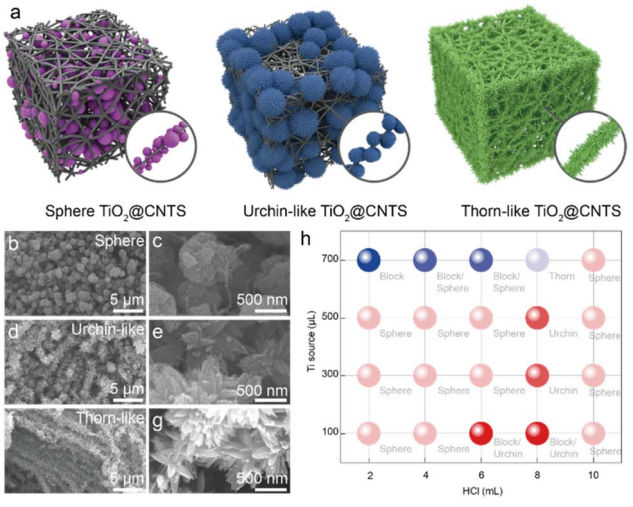

Fig. 1 Morphologies of TiO_2@CNTS composites. (a) A schematic illustration of the TiO_2@CNTS composites. (b and c) SEM images of the spherical TiO_2@CNTS composite. (d and e) SEM images of the urchin-like TiO_2@CNTS composite. (f and g) SEM images of the thorn-like TiO_2@CNTS composite. (h) A morphological phase diagram of TiO_2 *vs.* HCl concentration.

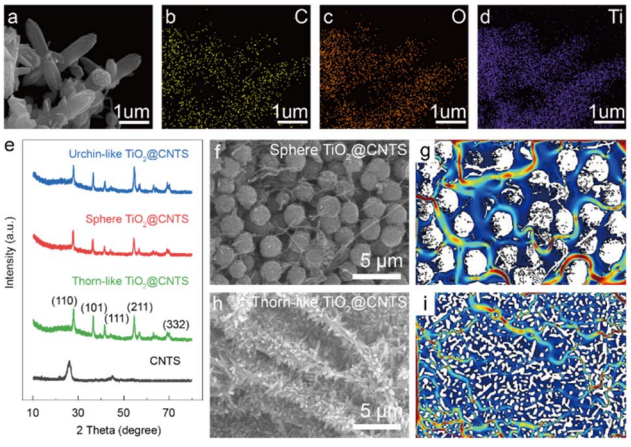

Fig. 2 Characterization of the TiO_2@CNTS composites. (a–d) EDS mapping of the thorn-like TiO_2@CNTS composite. (e) X-ray diffraction (XRD) patterns of TiO_2@CNTS composites with different morphologies. (f) An SEM image of the spherical TiO_2@CNTS composite for mass transfer behavior simulations. (g) The simulation results for mass transfer behavior in the spherical TiO_2@CNTS composite. (h) An SEM image of the thorn-like TiO_2@CNTS composite for mass transfer behavior simulations. (i) The simulation results for mass transfer behavior in the thorn-like TiO_2@CNTS composite.

enhancement in the capacitance performance of the thorn-like TiO_2@CNTS sample.

Subsequently, we evaluated the electrochemical performances of spherical, urchin-like, and thorn-like TiO_2@CNTS composites with scan rates ranging from 10 mV s^{-1} to 50 mV s^{-1} (Fig. 3). The thorn-like TiO_2@CNTS composite exhibits specific capacitance of 52.4 mF cm^{-2}, increasing by 57.8% and 33.3% compared to the spherical and urchin-like samples, respectively. The diffusion-controlled capacitance percentages of the thorn-like TiO_2@CNTS composite were 36%, 29%, 25%, 21% and 19% at 10, 20, 30, 40, and 50 mV s^{-1}, while the spherical and urchin-like TiO_2@CNTS composites exhibit lower diffusion-controlled capacitance percentages, indicating an increase in the pseudocapacitive contribution for the thorn-like sample. The thorn-like TiO_2@CNTS composite also exhibited an increase of up to 100% in specific capacity compared to pristine CNTS.

The electrochemical performances of the TiO_2@CNTS composites exhibit significant morphology dependence (Fig. 4). The cyclic voltammetry (CV) curves (Fig. 4a) show that thorn-like TiO_2@CNTS possesses a smaller potential difference between the reduction and oxidation peaks at a scan rate of 10 mV s^{-1}, indicating faster interfacial charge transfer kinetics and lower polarization. Linear sweep voltammetry (LSV) tests (Fig. 4b) demonstrate that the TiO_2 coating effectively suppresses electrolyte decomposition, thereby broadening the stable potential window at the electrode/electrolyte interface. Galvanostatic charge–discharge (GCD) curves (Fig. 4c–e) confirm that

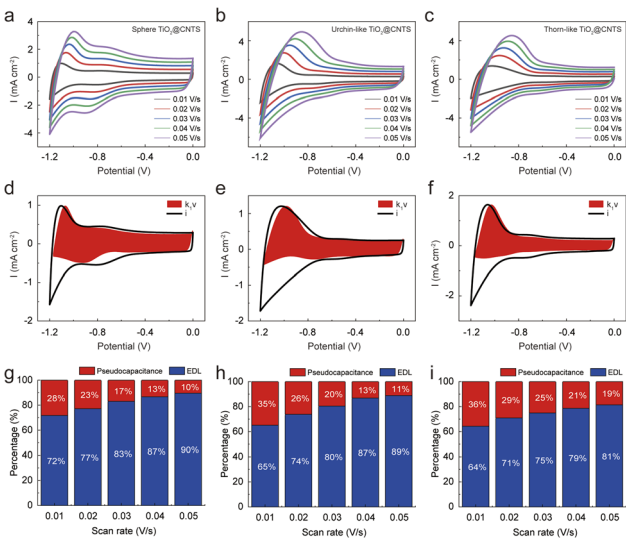

Fig. 3 Capacitive performances of TiO_2@CNTS composites with various morphologies. (a–c) Cyclic voltammetry (CV) curves of the spherical TiO_2@CNTS composite, urchin-like TiO_2@CNTS composite and thorn-like TiO_2@CNTS composite. (d–f) Pseudo-capacitance calculation results for the spherical TiO_2@CNTS composite, urchin-like TiO_2@CNTS composite and thorn-like TiO_2@CNTS composite. (g–i) The relative pseudo-capacitance and double layer contributions for the spherical TiO_2@CNTS composite, urchin-like TiO_2@CNTS composite and thorn-like TiO_2@CNTS composite at sweep speeds of 1–50 mV s^{-1}.

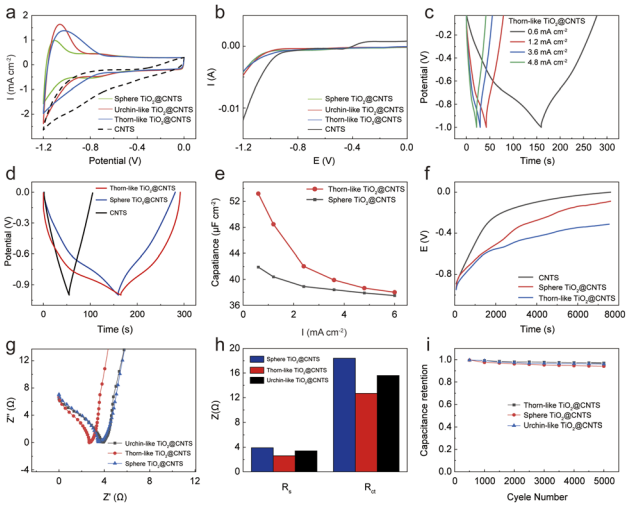

Fig. 4 A comparison of the charge and discharge performances of TiO_2@CNTS samples. (a) Cyclic voltammetry (CV) curves of CNTS (black line) and spherical (green line), urchin-like (red line) and thorn-like (blue line) TiO_2@CNTS composite electrodes. (b) Linear sweep voltammetry (LSV) curves of CNTS (black line) and spherical (green line), urchin-like (red line) and thorn-like (blue line) TiO_2@CNTS composite electrodes. (c) Galvanostatic charge–discharge (GCD) curves of thorn-like TiO_2@CNTS at different current densities. (d) GCD curves of CNTS, spherical TiO_2@CNTS and thorn-like TiO_2@CNTS at a sweep speed of 0.6 mA cm^{-2}. (e) The variation in area-specific capacitance of sphere-like TiO_2@CNTS and thorn-like TiO_2@CNTS as a function of scan rate. (f) A self-discharge comparison between spherical TiO_2@CNTS, thorn-like TiO_2@CNTS and pure CNTS electrodes. (g–i) Electrochemical impedance spectroscopy (EIS, g) analysis, equivalent series resistance (R_s) and charge transfer resistance (R_{ct}, h) values, and long-term cycling stability (i) of the TiO_2@CNTS composite electrodes.

spherical TiO_2@CNTS exhibits superior rate capability (with capacity retention of 90% at a current density of 4.8 mA cm^{-2}), and its discharge time is significantly longer than that of pristine CNTS. Furthermore, the self-discharge rate of TiO_2@CNTS is markedly reduced (Fig. 4f); due to improved wettability and optimized ion transport kinetics, its half-voltage time is extended to approximately 2500 seconds. Electrochemical impedance spectroscopy (EIS) analysis (Fig. 4g and h) reveals that the thorn-like TiO_2@CNTS composite electrode possesses significantly lower charge transfer resistance (R_{ct}) and series resistance (R_s). Finally, thorn-like TiO_2@CNTS maintains capacity retention of 97% after 5000 cycles (Fig. 4i), highlighting the exceptional structural stability conferred by the enhanced integration of thorn-like TiO_2 within the three-dimensional CNTS framework.

In this study, TiO_2 nanostructures with different morphologies were successfully incorporated into carbon nanotube sponges (CNTSs) using a simple hydrothermal method. Both experimental and simulation results indicate that the introduction of TiO_2 significantly enhances the hydrophilicity of the electrode and increases the effective solid–liquid contact area, thereby optimizing the fluid-related behaviors (infiltration and ion transport) of the electrolyte. Among them, the thorn-like TiO_2@CNTS composite exhibits superior nanochannel and

interfacial characteristics, demonstrating a 250% increase in area-specific capacitance compared to pristine CNTS, along with improved rate performance and cycling stability. This work reveals the intrinsic relationship between electrode nanostructure, electrolyte fluid behavior, and energy storage performance, providing clear insights for the design of next-generation high-performance supercapacitors. Furthermore, these structure-mediated design principles, specifically the transition from isotropic to anisotropic thorn-like geometry, offer a universal strategy to optimize electrolyte fluid behavior and electrochemical performance in other transition-metal-oxide systems, such as MnO_2 and V_2O_5.

Author contributions

Heping Cao: conceptualization, methodology, hydrothermal synthesis, characterization, writing – original draft. Chengqing Tang: methodology, mass transfer behavior simulations, electrochemical performance evaluation, writing – original draft. Jiashuo Duan: data curation, chemical analysis (XRD and EDS mapping). Zhaohui Yang: conceptualization, supervision, validation, writing – review & editing. Yitan Li: conceptualization, project administration, supervision, validation, writing – review & editing.

Conflicts of interest

There are no conflicts to declare.

Data availability

The data supporting this article have been included as part of the supplementary information (SI). Supplementary information: SEM images, FT-IR spectra, water contact angle test data, CMOSOL visualization diagrams, and electrochemical performance data. See DOI: https://doi.org/10.1039/d6na00092d.

Acknowledgements

The National Natural Science Foundation of China (grant no. 22402103), the Program of Taishan Scholar (grant no. tsqn202312040), the Natural Science Foundation of Shandong Province (grant no. 2024HWYQ-011 and 2025KJHZ014), and the Natural Science Foundation of Jiangsu Province (grant no. BK20240418) are acknowledged.

References

1 K. Ren, Z. Liu, T. Wei and Z. Fan, Recent Developments of Transition Metal Compounds-Carbon Hybrid Electrodes for High Energy/Power Supercapacitors, *Nano-Micro Lett.*, 2021, **13**(1), 129.
2 S. A. Ansari, N. Parveen, M. Z. Ansari, G. M. Alsulaim, M. W. Alam, M. Y. Khan, A. Umar, I. Hussain and K. Zhang, Exploring recent advances in the versatility and efficiency of carbon materials for next generation supercapacitor applications: A comprehensive review, *Prog. Mater. Sci.*, 2025, **154**, 101493.
3 H. Xue, P.-H. Huang, L.-L. Lai, Y. Su, A. Strömberg, G. Cao, Y. Fan, S. Khartsev, M. Göthelid, Y.-T. Sun, J. Weissenrieder, K. B. Gylfason, F. Niklaus and J. Li, High-rate metal-free MXene microsupercapacitors on paper substrates, *Carbon Energy*, 2024, **6**(5), e442.
4 A. Perju, D. Zhang, R. J. Wang, P.-L. Taberna, Y. Gogotsi and P. Simon, Operando Tracking of Resistance, Thickness, and Mass of Ti3C2Tx MXene in Water-in-Salt Electrolyte, *Adv. Energy Mater.*, 2025, **15**(20), 2405028.
5 M. Gao, Z. Wang, Z. Liu, Y. Huang, F. Wang, M. Wang, S. Yang, J. Li, J. Liu, H. Qi, P. Zhang, X. Lu and X. Feng, 2D Conjugated Metal–Organic Frameworks Embedded with Iodine for High-Performance Ammonium-Ion Hybrid Supercapacitors, *Adv. Mater.*, 2023, **35**(41), 2305575.
6 D. Wu, Y. Zhang, Z. Man, H. Zhang, X. Zhu, J. Ding, J. Xu, N. Bao and W. Lu, In Situ Fabrication of Graphdiyne Nanoisland Anchored Ti3C2Tx Film to Accelerate Intercalation Pseudocapacitance Kinetics, *Adv. Energy Mater.*, 2024, **14**(18), 2304404.
7 Y. Liu, C. Yu, S. Lan, W. Liu and J. Qiu, Microscopic-Level Anion & Diluent Chemistry in Electrolyte for Aqueous Supercapacitors Operating at High Voltage and Low Temperature, *Adv. Mater.*, 2025, **37**(35), 2503157.
8 J. Dai, C. Yang, Y. Xu, X. Wang, S. Yang, D. Li, L. Luo, L. Xia, J. Li, X. Qi, A. Cabot and L. Dai, MoS2@Polyaniline for Aqueous Ammonium-Ion Supercapacitors, *Adv. Mater.*, 2023, **35**(39), 2303732.
9 P. Simon, Y. Gogotsi and B. Dunn, Where Do Batteries End and Supercapacitors Begin?, *Science*, 2014, **343**(6176), 1210–1211.
10 T. Xu, Z. Li, D. Wang, M. Zhang, L. Ai, Z. Chen, J. Zhang, X. Zhang and L. Shen, A Fast Proton-Induced Pseudocapacitive Supercapacitor with High Energy and Power Density, *Adv. Funct. Mater.*, 2022, **32**(5), 2107720.
11 S. Arya, A. Singh, A. Ahmed, B. Padha, A. Banotra, U. Parihar, A. K. Sundramoorthy, S. Dixit and N. I. Vatin, Energizing tomorrow: The potential of light-driven supercapacitors in future applications, *J. Energy Chem.*, 2025, **105**, 193–223.
12 N. A. Wadodkar, R. S. Salunke, S. K. Pawar, A. Umar, A. A. Ibrahim, S. Akbar, S. A. Ansari, S. Baskoutas and D. J. Shirale, Next-Generation Supercapacitors: Advances in Binder-Free Electrodes, Scalable Fabrication, and Emerging Applications, *Adv. Sustainable Syst.*, 2026, **10**(1), e00599.
13 M. Salanne, B. Rotenberg, K. Naoi, K. Kaneko, P. L. Taberna, C. P. Grey, B. Dunn and P. Simon, Efficient storage mechanisms for building better supercapacitors, *Nat. Energy*, 2016, **1**(6), 16070.
14 L. Zhao, Y. Li, M. Yu, Y. Peng and F. Ran, Electrolyte-Wettability Issues and Challenges of Electrode Materials in Electrochemical Energy Storage, Energy Conversion, and Beyond, *Adv. Sci.*, 2023, **10**(17), 2300283.
15 P. Simon and Y. Gogotsi, Perspectives for electrochemical capacitors and related devices, *Nat. Mater.*, 2020, **19**(11), 1151–1163.

16 T. Nguyen and M. d. F. Montemor, Metal Oxide and Hydroxide–Based Aqueous Supercapacitors: From Charge Storage Mechanisms and Functional Electrode Engineering to Need-Tailored Devices, *Adv. Sci.*, 2019, **6**(9), 1801797.
17 A. Zhang, Z. Bi, G. Wang, S. Liao, P. Das, H. Lin, M. Li, Y. Yu, X. Feng, X. Bao and Z.-S. Wu, Regulating electrode/electrolyte interfacial chemistry enables 4.6 V ultra-stable fast charging of commercial LiCoO2, *Energy Environ. Sci.*, 2024, **17**(9), 3021–3031.
18 A. Daraghmeh, S. Hussain, A. U. Haq, I. Saadeddin, L. Servera and J. M. Ruiz, Carbon nanocomposite electrodes for electrical double layer capacitor, *J. Energy Storage*, 2020, **32**, 101798.
19 A. G. Olabi, Q. Abbas, A. Al Makky and M. A. Abdelkareem, Supercapacitors as next generation energy storage devices: Properties and applications, *Energy*, 2022, **248**, 123617.
20 P. Simon and Y. Gogotsi, Materials for electrochemical capacitors, *Nat. Mater.*, 2008, **7**(11), 845–854.
21 M. T. Islam, B. Gollas and Q. Abbas, Differentiating ion transport of water-in-salt electrolytes within micro- and meso-pores of a multiporous carbon electrode, *J. Mater. Chem. A*, 2024, **12**(37), 25504–25518.
22 Y. Wu, Y. Qian, B. Niu, J. Chen, X. He, L. Yang, X.-Y. Kong, Y. Zhao, X. Lin, T. Zhou, L. Jiang and L. Wen, Surface Charge Regulated Asymmetric Ion Transport in Nanoconfined Space, *Small*, 2021, **17**(28), 2101099.
23 V. Augustyn, J. Come, M. A. Lowe, J. W. Kim, P.-L. Taberna, S. H. Tolbert, H. D. Abruña, P. Simon and B. Dunn, High-rate electrochemical energy storage through Li+ intercalation pseudocapacitance, *Nat. Mater.*, 2013, **12**(6), 518–522.
24 C. Largeot, C. Portet, J. Chmiola, P.-L. Taberna, Y. Gogotsi and P. Simon, Relation between the Ion Size and Pore Size for an Electric Double-Layer Capacitor, *J. Am. Chem. Soc.*, 2008, **130**(9), 2730–2731.
25 L. L. Zhang and X. S. Zhao, Carbon-based materials as supercapacitor electrodes, *Chem. Soc. Rev.*, 2009, **38**(9), 2520–2531.
26 X. Gui, J. Wei, K. Wang, A. Cao, H. Zhu, Y. Jia, Q. Shu and D. Wu, Carbon Nanotube Sponges, *Adv. Mater.*, 2010, **22**(5), 617–621.
27 C. Tang, S. Zhang, J. Zhang, X. Zhang, Z. Hang, Y. Li and Z. Yang, Silicon carbide coated carbon nanotube porous sponge with super Elasticity, low Density, high thermal Resistivity, and synergistically enhanced electromagnetic interference shielding performances, *Chem. Eng. J.*, 2023, **469**, 144011.
28 B. Yang, W. Zhao, Z. Gao, J. Yang, W. Shi, Y. Zhang, Q. Su, B. Xu and G. Du, Flexible CNT@Porous carbon sponge cathode with large mesopores for high-rate zinc-ion hybrid capacitors, *Carbon*, 2024, **218**, 118695.
29 Z. Song, L. Miao, Y. Lv, L. Gan and M. Liu, Versatile carbon superstructures for energy storage, *J. Mater. Chem. A*, 2023, **11**(24), 12434–12455.
30 N. A. Wadodkar, R. S. Salunke, S. K. Pawar, A. Umar, A. A. Ibrahim, S. Akbar, S. A. Ansari, S. Baskoutas and D. J. Shirale, Next-Generation Supercapacitors: Advances in Binder-Free Electrodes, Scalable Fabrication, and Emerging Applications, *Adv. Sustainable Syst.*, 2026, **10**(58), e00599.
31 J. Sun, S. Li, Y. Li, X. Zhang and Z. Yang, High-Performance Flexible Asymmetric Supercapacitor Based on Nanostructured MnO2 and Bi2O3 Decorated 3D Carbon Nanotube Sponge in an Aqueous Gel-Electrolyte, *ACS Appl. Energy Mater.*, 2024, **7**(17), 7450–7458.
32 Y.-M. Wei, K. D. Kumar, L. Zhang and J.-F. Li, Pseudocapacitive materials for energy storage: properties, mechanisms, and applications in supercapacitors and batteries, *Front. Chem.*, 2025, 13–2025.
33 L. Chen, B. Tu, X. Lu, F. Li, L. Jiang, M. Antonietti and K. Xiao, Unidirectional ion transport in nanoporous carbon membranes with a hierarchical pore architecture, *Nat. Commun.*, 2021, **12**(1), 4650.
34 B. Sun, T. Shi, Z. Peng, W. Sheng, T. Jiang and G. Liao, Controlled fabrication of Sn/TiO2 nanorods for photoelectrochemical water splitting, *Nanoscale Res. Lett.*, 2013, **8**(1), 462.
35 S. Yang, Y. Lin, X. Song, P. Zhang and L. Gao, Covalently Coupled Ultrafine H-TiO_2 Nanocrystals/Nitrogen-Doped Graphene Hybrid Materials for High-Performance Supercapacitor, *ACS Appl. Mater. Interfaces*, 2015, **7**(32), 17884–17892.